O^- dynamic Jahn-Teller polarons in $KTaO_3$

EUROPHYSICS LETTERS 15 December 2003

Europhys. Lett., **64** (6), pp. 776–782 (2003)

O^- dynamic Jahn-Teller polarons in $KTaO_3$

M. Maiwald and O. F. Schirmer(*)

Fachbereich Physik, Universität Osnabrück - D-49069 Osnabrück, Germany

(received 16 June 2003; accepted in final form 15 October 2003)

PACS. 71.38.Ht – Self-trapped or small polarons.
PACS. 71.70.Ej – Spin-orbit coupling, Zeeman and Stark splitting, Jahn-Teller effect.

Abstract. – It is analyzed how dynamic Jahn-Teller coupling of an O^- hole with the surrounding lattice in oxide perovskites affects the electron paramagnetic resonance of shallow O^- defects. The predicted unusual resonance parameters are seen to be realized by experimentally identified O^- defects in $KTaO_3$. These centers thus manifest the properties of dynamic Jahn-Teller hole polarons in oxide perovskites. By varying the strength of the Jahn-Teller coupling, a continuous transition to the static Jahn-Teller case is modelled. The latter situation describes the properties of O^- polarons identified previously in other oxide perovskites.

The oxygen p_π-orbitals in the oxide perovskites (OP) are twofold degenerate (fig. 1). Since mainly such states form the upper edge of the valence bands of the OP, holes created by suitable illumination or by doping tend to populate such orbitals. Because of their degeneracy, a Jahn-Teller stabilization of the holes is expected. To find free oxygen holes in the thermal ground state is unlikely, however, since acceptor defects, always present as unintended background impurities or by doping, will trap them. Examples are O^- ions next to Al_{Ti} in $SrTiO_3$ [1] or O^- neighboring Na_{Ba} in $BaTiO_3$ [2]. Coupling of the hole to the lattice usually affects the structure of such O^- centers in two ways: First, it breaks the equivalence of the oxygen sites next to the acceptor ion, localizing the hole typically at one of the six O^{2-} ions next to an acceptor at a B-site, *e.g.* Al, or at one of the twelve O^{2-} ions next to an A-site acceptor, *e.g.* Na. This corresponds to the formation of a small hole polaron, bound to an acceptor. Second, the Jahn-Teller interaction tends to lift the twofold orbital degeneracy at each of these local potential hole sites, supporting the hole localization. The resulting charge carrier is labelled "Jahn-Teller polaron", since the polaron at each of its possible sites has an internal structure of Jahn-Teller interacting degenerate orbitals [3].

For the mentioned two O^- sample cases the Jahn-Teller effect was identified to be static, as indicated by a breaking of the local symmetries at each of the potential polaron sites from axial (fig. 1) to orthorhombic. This means that one of the two degenerate p_π-orbitals has become the ground state. Here we report the identification of shallow bound dynamic O^- Jahn-Teller polarons in $KTaO_3$, where the local tetragonal symmetry is not broken, although there is still a sizeable Jahn-Teller interaction. In spite of this, the competition between local-symmetry breaking of this type and symmetry conservation by spin-orbit coupling is decided in favor of the latter. This manifests a so far unknown polaron structure of the oxygen valence states of the OPs.

(*) E-mail: schirmer@uos.de

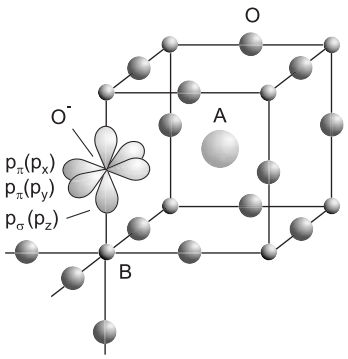

Fig. 1

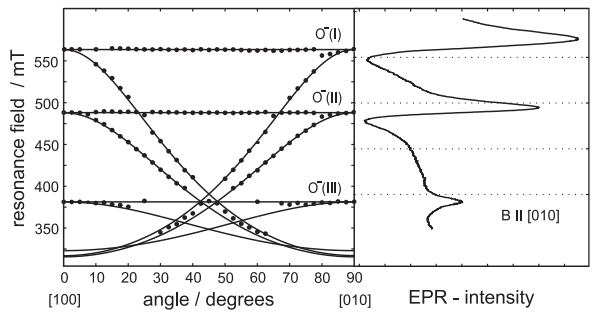

Fig. 2

Fig. 1 – An O^- ion in an ABO_3 oxide perovskite has axial symmetry with singly degenerate p_σ- and doubly degenerate p_π-orbitals. A possible acceptor at A is surrounded by twelve equivalent O^{2-} ions at B by six such ions.

Fig. 2 – Angular dependence of the resonance field positions of the O^- centers I, II and III in $KTaO_3$ for a microwave frequency 9.22 GHz ($T = 5$ K). Corresponding EPR signals are shown on the right.

For both cases, whether the local JT situation is static or dynamic, the point symmetry of the cluster of oxygen ions around an acceptor ion is broken by the localization of a hole at one of the equivalent O^{2-} members of the cluster. Jahn-Teller polarons breaking the translation symmetry of a crystal have been discussed in recent years as possible causes of high-temperature superconductivity, HTSC [4] and colossal magnetoresistance, CMR [5]. Electron paramagnetic resonance (EPR) studies have clarified the microscopic structure of Ti^{3+} conduction Jahn-Teller polarons in $BaTiO_3$ [6]. Since the coupling of carriers to the lattice is specific to several properties of the OP, including HTSC and CMR, it is important to gain further experience on how such interactions can express themselves, as, *e.g.*, by the new dynamic manifestation of a vibronic state of a trapped hole.

Information on the structural properties of the O^- trapped polarons treated here is also taken from EPR studies. While the static Jahn-Teller effect expresses itself by an orthorhombic g-tensor (table I), the dynamic situation encountered for $KTaO_3$ is characterized by an axial one, *i.e.* by a lattice coupling conserving axial symmetry (table I). Three such centers of similar axial structure (fig. 2, table I) have been identified. These have first been observed by Laguta *et al.* [7], who attributed them initially to Ta^{4+}, slightly perturbed by three different unknown defect associations. This assignment to Ta^{4+} ($5d^1$) was prompted by the strongly

Table I – *Zeeman, crystal-field and Jahn-Teller parameters of the treated* O^- *centers. The symmetry of the mentioned center* O^- *next to* Al_{Ti} *in* $SrTiO_3$ *is initially distorted along* $\langle 100\rangle$*-type crystal directions by the low-temperature rotation of the oxygen octahedra in* $SrTiO_3$*. Therefore, this system is less typical for the JT distortions along* $\langle 110\rangle$*-type directions of the OPs.*

	$g_{\|\|}(g_{100})$	$g_\perp(g_{1-10})$	$g_\perp(g_{110})$	E/cm^{-1}	g_l	$E_{\mathrm{JT}}/\mathrm{cm}^{-1}$	Reference
$BaTiO_3$:Na	2.0962	2.0077	1.9998	1600	1	(*)	[2]
$KTaO_3$ I	2.08	1.17	1.17	54	0.048	610	[7,8]
$KTaO_3$ II	2.09	1.35	1.35	68	0.059	570	[7,8]
$KTaO_3$ III	2.04	1.73	1.73	129	0.037	660	[7,8]

(*)The JT influence cannot be separated from the Na defect orthorhombicity, see, *e.g.*, eq. (5).

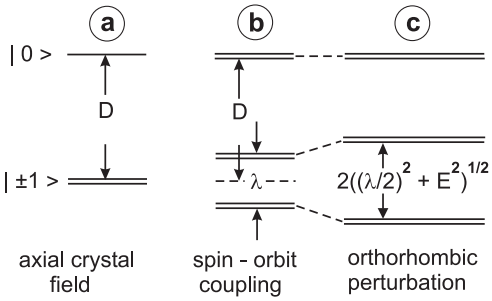

Fig. 3 – Energy levels of O^- $2p$-states under the indicated perturbations.

negative deviations of the $g_\perp$ parameters (table I) from the free-electron value, $g_s = 2.0$. Such "negative g-shifts" are usually assumed to be typical for single-electron systems such as Ta^{4+}, whereas O^- centers have been thought to be exclusively characterized by slightly "positive g-shifts". In contrast to the previous assignment, several experimental facts, *e.g.* the conditions under which the centers are created by illumination, required [8] to attribute these signals to O^- holes trapped at a shallow level about 80 meV above the valence band edge. This assignment was recently corroborated by Laguta *et al.* [9] on the basis of indirect evidence derived from the kinetics of light-induced conductivity and luminescence properties and their decay. In the present contribution we establish a microscopic model which allows to prove this assignment to O^- directly by the interpretation of its rather unusual EPR parameters. In spite of their different local symmetries, both static and dynamic O^- centers will be shown to represent boundary cases of the same type of defects.

O^- ($2p^5$) ions have orbital angular momentum $L = 1$ and spin $S = 1/2$. At each of the six (or twelve) potential small polaron sites, the O^- p-orbitals (fig. 1) have the level structure indicated in fig. 3a: a twofold degenerate O^- p_π ground state as well as a non-degenerate p_s level, lying higher by several electronvolts, as caused by the strong axial crystal-field splitting. This is expressed by the Hamiltonian $H_{\rm ax} = D(1 - L_z^2)$. O^- spin-orbit coupling, $H_{\rm so} = \lambda \boldsymbol{L}\boldsymbol{S}$, leads to a corresponding ground-state splitting, fig. 3b. The total Hamiltonian, $H = H_{\rm ax} + H_{\rm so}$, represented in the spin-orbit basis $|\pm 1^\pm\rangle = \frac{1}{\sqrt{2}}(|p_x^\pm\rangle \pm i|p_y^\pm\rangle)$ and $|0^\pm\rangle = |p_z^\pm\rangle$, where the superscripts indicate the spin-projections, has the structure

$$\begin{matrix} |\mp 1^\mp\rangle \\ |\pm 1^\pm\rangle \\ |0^\pm\rangle \end{matrix} \begin{pmatrix} \lambda/2 & 0 & 0 \\ 0 & -\lambda/2 & \lambda/\sqrt{2} \\ 0 & \lambda/\sqrt{2} & D \end{pmatrix}. \tag{1}$$

The two time conjugate basis sets indicated on the left lead to identical matrices. Because the axial energy splitting D is much larger, about four eV [10], than λ ($\lambda_{O^-} \sim 20$ meV), the off-diagonal elements can be neglected. The experimental EPR results have to be compared to those predicted from a calculation of the Zeeman effect of the ground state in fig. 3b. It is derived by operating with $H_{\rm Zee} = \mu_{\rm B}\boldsymbol{B}(g_L\boldsymbol{L} + g_s\boldsymbol{S})$ on this state. For a free O^- ion the orbital g-value, g_L, is equal to 1; as will be shown, it can be strongly modified to an effective value, g_l, by a dynamic Jahn-Teller coupling.

In order to take account of a possible orthorhombicity, which usually characterizes the O^- centers in the OP, the term $H_{\rm orth} = E(L_x^2 - L_y^2)$, has to be added to the Hamiltonian. This mixes the p_π-states $|1\rangle$ and $|-1\rangle$ and leads to the level splitting shown in fig. 3c. This level scheme as well as its Zeeman effect is isomorphous to that of the O_2^- molecule in alkali halides, treated by Zeller and Känzig [11]. They calculate the following principal g-values, to

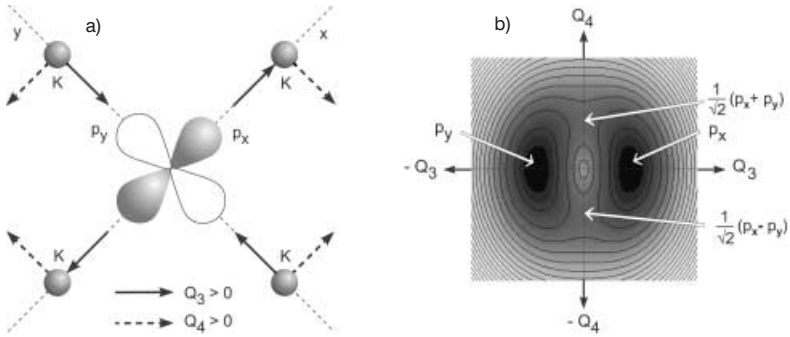

Fig. 4 – a) Vibrational excursions in the O-K cluster corresponding to the Q_3 and Q_4 modes coupling to the p_π-states. As shown, the arrows indicate the stabilization of p_x as the hole ground state. b) Lower-energy sheet of the eigenvalues of the JT Hamiltonian in the Q_3, Q_4 space, calculated with the parameters $\nu_3 = 1$, $\nu_4 = 0.5$, $K_3 = 2$, $K_4 = 1$. The electronic eigenstates at the various locations in the Q_3, Q_4 space are indicated.

be measured for $\boldsymbol{B}$ along the principal directions indicated by the subscripts:

$$g_{110} = g_s \cos\vartheta - g_L(\lambda/D)(\cos\vartheta + 1 - \sin\vartheta), \tag{2a}$$

$$g_{1\text{–}10} = g_s \cos\vartheta - g_L(\lambda/D)(\cos\vartheta - 1 + \sin\vartheta), \tag{2b}$$

$$g_{001} = g_s + 2g_L \sin\vartheta \tag{2c}$$

with $\tan\vartheta = \lambda/2E$.

Here the last terms in eqs. (2a) and (2b) result from the orbital angular-momentum operators L_x and L_y in the Zeeman Hamiltonian. They contribute only via spin-orbit admixture of the state $|0\rangle$ to the $|1\rangle$ and $|-1\rangle$ orbitals. Therefore, they are multiplied by the small factor λ/D. The operator L_z, on the other hand, contributes in first order (eq. (2c)).

Equations (2) can be specialized to the case that the hole "rotates" in an unimpeded way around the axis of the center (fig. 4a); then the axial symmetry is not broken and $E = 0$. This means that $\vartheta = \pi/2$ and the following principal values of the g-tensor are expected:

$$g_{110} = g_{1\text{–}10} = g_\perp = 0 \quad \text{and} \quad g_{001} = g_{||} = 2g_L + g_s = 4 \tag{3}$$

for $g_L = 1$. The measured values (table I) clearly deviate from this prediction. However, a slight orthorhombic perturbation, $E \neq 0$, as well as an orbital g-value, $g_l \neq g_L$, much smaller than 1 in eq. (2c), can explain the experimental data. The possible origin of this influence will be discussed farther below, while the small value of g_l will be attributed to a dynamic Jahn-Teller effect in the next section. It will furthermore be shown that the observed Zeeman effect will be effectively axially symmetric, in spite of the assumed orthorhombicity. Now the experimentally determined g-values can be reproduced, using the values of E and g_l shown in table I. It is seen that rather small orthorhombic influences lead to this result.

In order to explain the small value of g_l and the axial symmetry of the centers, we suppose that a dynamic version of the JTE is active. Here we can rely on a similar sample case presented by Estle [12] as an introduction to the JTE. He showed that only the two cluster vibration modes Q_3 and Q_4, depicted in fig. 4a, can couple to the p_π-orbitals. Since the Q_4 excursions are tangential to the bond directions, their JT coupling is expected to be weaker than that of the Q_3 vibrations. Quantifying Estle's heuristic arguments [12], we obtain the JT Hamiltonian $H_{\mathrm{JT}} = \nu_3 E_3 Q_3 + \nu_4 E_4 Q_4 + H_{Q3} + H_{Q4}$. Here E_3 and E_4 are the electronic operators, acting on the p_x, p_y basis; they are given by $E_3 = \left(\begin{smallmatrix} 1 & 0 \\ 0 & -1 \end{smallmatrix}\right)$ and $E_4 = \left(\begin{smallmatrix} 0 & 1 \\ 1 & 0 \end{smallmatrix}\right)$, as listed,

e.g., for the prevailing D_{4h} symmetry in the tables of Koster *et al.* [13]. The parameters ν_3 and ν_4 represent the relevant coupling strengths. H_{Q_3} and H_{Q_4} indicate the Hamiltonians of the corresponding vibrations: $H_i = \frac{1}{2}K_iQ_i^2 + \frac{1}{2}\mu_iP_i^2$ $(i = Q_3, Q_4)$, where the P_i are the momenta conjugate to the Q_i. The eigenvalues of the H_i will be called $\varepsilon_{\mathrm{vib},i}$ and their eigenstates, $\chi(Q_i)$. For the static case ($P_i = 0$) the energy contours of H_{JT} in the Q_3, Q_4 space are derived from the diagonalization of H_{JT}:

$$E_{\pm} = \pm\left(\nu_4^2Q_4^2 + \nu_3^2Q_3^2\right)^{1/2} + 1/2K_4Q_4^2 + 1/2K_3Q_3^2. \tag{4}$$

The lower sheet, indicated by the minus sign of this expression, is depicted in fig. 4b. It visualizes that the ground-state orbital is p_x if $Q_3 > 0$ and p_y if $Q_3 < 0$. The parameters chosen for the presentation (see caption of fig. 4b) assume that the coupling to Q_3 is stronger than to Q_4, as expected.

Since the p_σ-orbitals are separated by the large axial crystal-field splitting D from the p_π-states, it is useful to consider the total Hamiltonian $H = H_{\mathrm{ax}} + H_{\mathrm{so}} + H_{\mathrm{orth}} + H_{\mathrm{JT}}$ only in the subspace spanned by p_x and p_y. In the basis $|p_x^{\pm}\rangle$, $|p_y^{\pm}\rangle$ it has the form

$$\begin{matrix} \\ |p_x^{\pm}\rangle \\ |p_y^{\pm}\rangle \end{matrix} \begin{matrix} \begin{matrix} \qquad\qquad\qquad\quad & \qquad\qquad\qquad\quad \end{matrix} \\ \begin{pmatrix} E + \nu_3Q_3 + \varepsilon_{\mathrm{vib},3} + \varepsilon_{\mathrm{vib},4} & \mp i\lambda/2 + \nu_4Q_4 \\ \pm i\lambda/2 + \nu_4Q_4 & -E - \nu_3Q_3 + \varepsilon_{\mathrm{vib},3} + \varepsilon_{\mathrm{vib},4} \end{pmatrix} \end{matrix}. \tag{5}$$

It is seen that the operators $E(L_x^2 - L_y^2)$ and $\nu_3E_3Q_3$ are diagonal, $\nu_4E_4Q_4$ and λL_zS_z off-diagonal. The operators L_x and L_y are coupling the $p_\pi(p_x, p_y)$ orbitals in the subspace to the $p_\sigma(p_z)$ state outside of this space. They thus do not contribute to eq. (5); the admixture of the excited orbital to the ground state is furthermore reduced by the small ratio λ/D. If only coupling to the Q_3 vibrations is taken into account and the weaker interaction with the Q_4 modes neglected, the p_π-vibronic states are $p_x\chi(Q_3)$ and $p_y\chi(-Q_3)$, where χ represents the ground states of the Q_3 vibration. All off-diagonal matrix elements in eq. (5) are now reduced [14] by the vibrational-overlap integral $\langle\chi(Q_3) \mid \chi(-Q_3)\rangle$, see eq. (6). Since the corresponding vibrations occur in the two-well potential along the Q_3 coordinate in fig. 4b, one calculates $\langle\chi(Q_3) \mid \chi(-Q_3)\rangle = \exp[-4E_{\mathrm{JT}}/\hbar\omega] = r$; such vibrational overlaps of two displaced oscillators are valid, as in ref. [14], for all coupling strengths [15]. E_{JT} is the energy decrease by vibronic interaction with only a Q_3 mode and $\hbar\omega$, the energy of a representative vibration. In particular, it follows that the spin-orbit coupling, being off-diagonal in eq. (5), is reduced by r. Furthermore, the coupling to the Q_4 vibration is decreased by the same factor. This means that the influence of Q_4 is further quenched, once the reasonable assumption has been made that coupling to Q_3 is dominating.

Now the matrix elements of the orbital Zeeman operator, $H_{\mathrm{Zee},L} = \mu_{\mathrm{B}}\boldsymbol{B}g_L\boldsymbol{L}$, will be calculated with the vibronic states $|p_x\rangle|\chi(Q_3)\rangle$ and $|p_y\rangle|\chi(-Q_3)\rangle$. As before, in the p_x, p_y subspace the largest matrix elements are those of L_z, because those of L_x and L_y are reduced by λ/D. We thus have

$$\begin{aligned} \langle g_l\mu_{\mathrm{B}}L_z\rangle &= \langle p_x\chi(Q_3)|g_L\mu_{\mathrm{B}}L_z|p_y\chi(-Q_3)\rangle \\ &= \langle p_x|g_L\mu_{\mathrm{B}}L_z|p_y\rangle\langle\chi(Q_3)|\chi(-Q_3)\rangle. \end{aligned} \tag{6}$$

It is seen that the orbital g-value, modified by Jahn-Teller coupling, g_l, is related to that of the uncoupled ion, $g_L = 1$, by $g_l = rg_L$. This scaling now allows to explain the g_l-values deduced from experiment via eq. (2), as listed in table I. Assuming coupling to a Q_3 mode with a representative vibration energy of 0.1 eV, the JT energies given in table I are derived. It should be noted that the orbital contributions to the g-tensor are reduced to the small

g_l-value only in eq. (2c), not in eqs. (2a) and (2c). In these cases, the matrix elements of L_x and L_y between the p_σ and p_π states enter, which are strongly non-degenerate and thus do not show any JT coupling. In principle, a further —orbital— reduction of $\langle L_z \rangle$ can occur, if the hole orbital ground state extends far from the O^- site towards its K^+ neighbors. This distance, however, is comparatively large (fig. 4). Therefore, it can be assumed safely that there is at most a rather modest admixture of K^+ orbitals to the ground state.

As shown above, the present dynamic hole centers have the outstanding feature that even a small non-axial perturbation can strongly influence the $g_\perp$-values (eqs. (2a) and (2c)) of the axial g-tensor: by increasing E, $g_\perp$ is shifted towards g_s, indicating an increased quenching of orbital angular momentum. We have tested this dependence of $g_\perp$ on the orthorhombicity by applying uniaxial stress perpendicular to the center axes. As expected, in this way the resonances move towards g_s. Also the highly unusual principal g-tensor values are characteristic for the dynamic JT system.

There are two observations which demonstrate that the dynamic and the static manifestations of the O^- systems rest on the same basis: The Zeeman effect of O^- at $BaTiO_3$:Na (table I) is interpreted [2] with the same spin-Hamiltonian, resulting in the above eqs. (2), as the present dynamic system. Furthermore, the study of O^- at $BaTiO_3$:Na revealed [2] that in this case the direction of the ground-state O^- p_π-orbital is not strictly fixed but rather librates around its mean, $\langle 110 \rangle$-type, direction. This can be considered to be the onset of a rotation, encountered to be less impeded in the present case; here, apparently, the symmetry-conserving spin-orbit interaction, off-diagonal in eq. (5), is more effective than the symmetry breaking hole-lattice coupling, diagonal in eq. (5).

There appears to be a contradiction between the observed axiality of the centers and the fact that some orthorhombicity has to be assumed to explain their features. However, the corresponding parameters E of the orthorhombic crystal field (table I) are so small that they do not influence the angular dependence of the spectra strongly. From eqs. (2a) and (2b) it is predicted that a possible orthorhombicity of the Zeeman splitting is represented by the term $\lambda/D \; g_L(1 - \sin\vartheta)$. The axial splitting d can be estimated from the energy distance between the highest p_σ —and the p_π— densities of state of the valence band of $KTaO_3$. An *ab initio* band structure calculation of $KTaO_3$ [10] leads to $D \sim 4\,\mathrm{eV}$. On this basis it is expected that, *e.g.*, the angular independent branches in fig. 2 cover a splitting of at most 0.75 mT. This splitting should be largest along the [110]-type directions, see eqs. (2). Since the total linewidth is about 25 mT, such a splitting cannot be resolved. The observed effective axiality thus is not in contradiction to the slight orthorhombic crystal field required by the model.

The consequences of a level ordering as in fig. 3c, leading to a g-tensor with strong negative shifts of g_{001} and a pronounced insensitivity to orthorhombic perturbation, have been identified before in the ground states of the Pt^- defect in Si [16] and of Ti^{3+} at a trigonal, slightly non-axially strained site in doped $CsAl(SO_4) \cdot 12H_2O$ [17].

The microscopic origin of the small orthorhombicities needed to reproduce the measured g parameters is not yet known for the $KTaO_3$ centers. The information available from the EPR investigations [7, 8] is not sufficient to deduce any knowledge on this problem. One might speculate that isoelectronic replacements of the K ions next to the O^- ion are causing the orthorhombicities. The structure of the relevant perturbations must be well defined, however, because the same three modifications (table I) of the dynamic O^- center always turn up, corresponding to three distinct values of E, independent of the sample investigated. The relative abundance of the three orthorhombicities represented by centers I, II and III, however, depends on the specific sample and its annealing treatments [8, 9].

In any case, the orthorhombic perturbation is very weak, if compared, *e.g.*, to that of $BaTiO_3$:Na (table I), and thus the O^- hole can be considered to be almost free. In this

context it can be remarked that a free O^- center of this type ($E = 0$) is likely to escape observation by EPR since in this case its $g_\perp$-value of zero (eq. (3)) either shifts the resonance to infinitely high magnetic fields or leads to a zero EPR transition moment. Anyway, since the vibronic structure of a hole at a shallow level is likely to represent that of a hole in the nearby band, the present study thus establishes a model expected for a free dynamic JT hole polaron in an oxide perovskite.

That the symmetry of the present centers remains effectively axial, is caused by the smallness of the parameter E. This can be traced to the fact that $KTaO_3$ is a quantum paraelectric [18], where the corresponding fluctuations tend to suppress deviations from cubic symmetry. Rotation of a p_π-orbital requires that the lattice surrounding O^- is distorted as little as possible. This situation is more likely to be met in the incipient ferroelectric $KTaO_3$, being cubic down to the lowest temperatures, than in ferroelectric perovskites, such as $BaTiO_3$. In the latter cases, the low symmetry of the host lattices can decisively lift the degeneracy of the O^- $2p_\pi$-orbitals, or these lattices are prone to facilitate large spontaneous distortions induced by a captured hole.

It should be remarked that the hole ground state in the cuprate superconductors, which have structural features similar to those of the perovskites, is of p_σ-type, connecting neighboring Cu^{2+} ions. This difference to the present case appears to be caused by the low charge of the Cu ions and the strong Cu–O covalency, leading to a sizeable dispersion of the p_σ-bands and thus p_σ electron density lying above the p_π density.

REFERENCES

[1] Schirmer O. F., Berlinger W. and Müller K. A., *Solid State Commun.*, **18** (1976) 1505.
[2] Varnhorst T., Schirmer O. F., Kröse H., Scharfschwerdt R. and Kool Th. W., *Phys. Rev. B*, **53** (1996) 116.
[3] Höck K. H., Nickisch H. and Thomas H., *Helv. Phys. Acta*, **56** (1983) 237.
[4] Müller K. A., *J. Supercond.*, **12** (1999) 3; Mihailovic D. and Kabanov V. V., *Phys. Rev. B*, **63** (2001) 054505.
[5] See, *e.g.*, Allen P. B. and Perebeinos V., *Phys. Rev. B*, **60** (1999) 10747.
[6] Lenjer S., Schirmer O. F., Hesse H. and Kool Th. W., *Phys. Rev. B*, **66** (2002) 165106.
[7] Laguta V. V., Zaritskii M. I., Glinchuk M. D., Bykov I. P., Rosa J. and Jastrabik L., *Phys. Rev. B*, **58** (1998) 156.
[8] Maiwald M., PhD Thesis, Osnabrueck (1999).
[9] Laguta V. V., Glinchuk M. D., Bykov I. P., Cremona A., Galinetto P., Giulotto E., Jastrabik L. and Rosa J., *J. Appl. Phys.*, **93** (2003) 6056.
[10] Deduced from a simulation of the valence band structure of oxide perovskites by Postnikov A., private communication.
[11] Zeller H. R. and Känzig W., *Helv. Phys. Acta*, **40** (1967) 845.
[12] Estle T. L., in *Optical Properties of Ions in Solids, NATO ASI, Ser. B*, Vol. **8**, edited by di Bartolo B. (Plenum, New York) 1974, pp. 419-448.
[13] Koster G. F., Dimmock J. O., Wheeler R. G. and Statz H., *Properties of the 32 Point Groups* (MIT Press, Cambridge, Mass.) 1963.
[14] Ham F. S., *Phys. Rev. A*, **138** (1965) 1727.
[15] Keil T., *Phys. Rev. A*, **140** (1965) 601.
[16] Anderson F. G., Ham F. S. and Watkins G. D., *Phys. Rev. B*, **45** (1992) 3287.
[17] Tregenna-Piggott P. L. W., Noble C. J. and Pilbrow J. R., *J. Chem. Phys.*, **113** (2000) 3289.
[18] Müller K. A. and Burkhard H., *Phys. Rev. B*, **19** (1979) 3593.